

## **Lateral Heterogeneity in the Upper Mantle beneath the Tibetan Plateau and its Surroundings from SS-S Travel Time Residuals**

I. G. Dricker and S. W. Roecker  
Department of Earth and Environmental Sciences  
Rensselaer Polytechnic Institute, Troy, NY, 12180

### **Abstract**

We use SS-S differential travel times to map the upper mantle structure of the Tibetan Plateau and its surroundings. New observations from analog stations in the former Soviet Union help to fill in gaps in the spatial coverage of previous studies, providing new data for eastern Tibet, the Kunlun range, and the Tarim Basin. The effects of crustal thickness variations, anisotropy, and global heterogeneity are evaluated and explicitly accounted for by incorporating results of previous studies and by ray tracing through a global 3D model. The resulting residuals suggest that, with the exception of the easternmost part of the plateau, Tibet is underlain almost entirely by lithosphere of normal to greater than normal thickness. In general there appear to be strong lateral gradients in wave speed between eastern and western Tibet. We find little evidence for low wave speeds under northern Tibet to the west of about 87° E. Instead, the average shear wave speeds in the upper 300 km of the mantle beneath this part of Tibet are about 0.5 km/s faster than those directly to the north beneath the Tarim basin. To some extent, these results support models of Tibetan dynamics in which the lithosphere underlying northern Tibet underplates the crust as opposed to those in which large portions of this lithosphere disappear by convection, subduction, or detachment. At the same time, the dominant east-west gradient in residuals suggests that 2D models inadequately explain the dynamics of all of Tibet.

### **Introduction**

The active tectonics of Asia are for the most part a consequence of the collision between India and Eurasia, which began some 40-50 million years ago [e.g., Fisher et al., 1971; McKenzie and Sclater, 1971; Molnar and Tapponnier, 1975] and continues at a rate of 40 to 55 mm/year [e.g., Patriat and Achache, 1984; DeMets, 1993]. Among the more spectacular effects of this collision is the Tibetan Plateau (Figure 1), which averages 5000 m in elevation over an area of about 2 million km<sup>2</sup>. These elevations are maintained by an anomalously thick crust, which at 70 km is roughly twice that of normal continental crust. While some fraction of convergence has been accommodated by lateral extrusion [e.g., Molnar and Tapponnier, 1977;

Tapponier et al., 1982], this enormous accumulation of crust clearly is a result of large-scale, north-south shortening. However, the evolution of the plateau and the nature of the dynamics involved are still poorly understood and a number of different scenarios have been proposed to explain them (Figure 2). For purposes of this study we divide these scenarios into “thin lithosphere models”, in which the sub-crustal lithosphere under part of Tibet, usually northern Tibet, is thinned or missing entirely, and “thick lithosphere models” in which Tibet is underlain by some normal to greater than normal thickness of sub-crustal lithosphere. Among the thick lithosphere models are the underthrust models [Argand, 1924; Ni and Barazangi, 1983; Zhao and Morgan, 1985] in which the Indian crust underplates the Eurasian crust while the Indian upper mantle either follows along or is supplanted by the Eurasian lithosphere, and the “accordion” models [Dewey and Bird, 1970; Dewey and Burke, 1973] in which shortening is uniformly distributed throughout the preexisting lithosphere. In the thin lithosphere models, asthenospheric upwelling under northern Tibet occurs either because of the retreat of the Eurasian lithosphere [Willett and Beaumont, 1994], a local delamination [Owens and Zandt, 1997; Kosarev et al., 1999], a convective removal of the Eurasian lithosphere [e.g., Houseman et al., 1981], or some hybrid combination of these scenarios [Zhao et al., 1996].

Our current view of the structure of the crust and upper mantle beneath Tibet and surrounding regions is based on a number of low resolution seismic studies that average structure over 100s of km, supplemented by a few high resolution studies that provide tantalizing glimpses of small scale heterogeneity that may or may not be reliably extrapolated to larger portions of the plateau. A trend that emerges from these studies is a first order lateral variation in elastic wave speeds beneath Tibet. Higher than average wave speeds are found in the far western part of the plateau, up to and including the Karakorum [e.g., Molnar and Chen, 1984; Molnar, 1990; Pandey et al., 1991], and in the southern part of the plateau [e.g., Holt and Wallace, 1990], while lower than average wave speeds are found in parts of north-central and north-eastern Tibet [e.g., Romanowicz, 1982; Barazangi and Ni, 1982; Brandon and Romanowicz, 1986; Zhao and Xie, 1993; McNamara et al., 1997; Wittlinger et al., 1996]. Generally speaking, a “low-north, high-south” view of elastic wave speeds would favor the thin lithosphere models. However, the generally uneven scale of resolution provided by these studies permits other interpretations.

A useful observation for interrogating upper mantle structure beneath remote areas at a scale length of several 10s of km is multi-bounce S waves that reflect in the area of interest. In

particular, SS-S travel time residuals have helped to constrain upper mantle structure in a number of studies [e.g., Grand and Helmburger, 1985; Sheehan and Solomon, 1991; Woodward and Masters, 1991; hereafter WM91]. The basic idea of SS-S is simple: to the extent that the main contributor to shear wave travel time anomalies is heterogeneity in the crust and uppermost mantle (to depths of about 300 km), travel times of SS will be most sensitive to structure near a (shallow) source and receiver, and doubly sensitive to the crust and upper mantle beneath the bounce point (since it goes up and down). At teleseismic distances, S and SS share virtually the same ray path in the upper mantle beneath the source and receiver, and hence the SS-S residuals are sensitive primarily to structure beneath the bounce point.

The SS-S technique previously has been applied to the Tibetan region by Lyon-Caen [1986] and Woodward and Molnar [1995; hereafter WM95]. Lyon-Caen [1986] used only four SS-S observations, but reported an enormous (up to 25 s) difference between Tibetan and Indian shield raypaths. She inferred that the mantle beneath Tibet must be unusually hot to cause the large delay in SS travel time. WM95 analyzed 147 SS-S travel times in the region, and inferred a large (9%) difference in shear wave speed between northern and southern Tibet.

In this study, we extend the WM95 investigation by adding SS-S observations derived from a network of analog stations operating within the former Soviet Union. The source-receiver geometries afforded by this network allow us to fill in some of the spatial gaps in the WM95 study, resulting in a more complete picture of the structure of the mantle beneath Tibet and surrounding regions. We also use recent models of local anisotropy and global heterogeneity to reevaluate the uncertainties in the interpretation of these observations.

### **Data**

The data used in this study are analog seismograms recorded at stations in the former Soviet Union between 1977 and 1995. Each station is equipped with three-component Kirnos SKD sensors. The response of the entire system is flat between periods of 1 and 20 s and magnification is about 1000. Timing accuracy is better than 0.1 s [Usenko, 1991]. Photosensitive paper records ground motion at 60 mm/min, and all three components are recorded simultaneously on the same seismogram.

Over the past several years we assembled copies of about 2000 seismograms from the archives of 14 of these seismic stations (Figure 3). Following techniques developed in previous studies using this type of data [e.g., Makeyeva et al., 1992; Vinnik et al., 1992;

Kosarev et al., 1993; Dricker et al., 1999], we scanned these seismograms and derived digital time series from the raster images. Digitized seismograms are compared directly with the original analogue records to ensure a reasonable level of fidelity.

For this study we selected seismograms of 421 event-station pairs in the 48 - 90 distance range for which the SS bounce points are within or near the Tibetan Plateau (Figure .3). This distance range is chosen to avoid interference with other phases and upper mantle triplications for both S and SS.

## **Analysis**

### *Generating Observed and 1D Predicted SS-S*

Because our principal observations are SS-S delay times, the first step in the analysis is to identify the S and SS phases on the digitized seismograms. We begin by rotating the horizontal components into the transverse and radial frame using the theoretical back azimuth. Only the transverse (SH) components are used in order to minimize the effect of S-to-P conversions and a possible contamination by the SKS phase at distances near 80°. We then select the waveforms using a 120 s window about the theoretical arrival times, and taper these windows with a cosine to reduce edge effects. We experimented with low-pass filters of various corner frequencies (0.2, 0.1, and 0.06 Hz) but found that filtering has no significant effect on the results. To identify the SS phase, we follow the procedure of previous investigators (e.g., WM91) and use the Hilbert transform of the S phase as an approximation of the teleseismic SS [Choy and Richards, 1975] and allow for differences in attenuation by applying a  $t^*$  of 3 s to the direct phase. The transformed S phase is then cross-correlated with the SS window to obtain the best estimate of SS-S for the station-event pair.

A predicted SS-S is generated using the Preliminary Reference Earth Model (PREM) [Dziewonski and Anderson, 1981] with appropriate corrections for ellipticity [Dziewonski and Gilbert, 1976], and the resulting differential time residual ( $DTR = [SS-S]_{obs} - [SS-S]_{calc}$ ) is plotted at the PREM bounce point (the midpoint of the great circle between source and receiver after correcting for source depth). We use PREM because it was the reference model of previous studies [WM91, WM95] and hence comparison with those studies is facilitated. Note that positive DTRs correspond to lower than normal shear wave speeds, and negative DTRs to higher than normal wave speeds.

### *Quality control*

The large variation in the 421 DTRs derived using the procedure described above, even for source-receiver pairs in the same location, suggests that the data quality is uneven, and therefore considerable effort was spent to identify and remove probable outliers. We began by establishing retention criteria based on the ability of the cross correlation operation to identify an SS from a transformed S. A low value for a cross correlation maximum is an obvious indicator, and we set a minimum of 0.5 for retention. We also found that in several cases the correlation function had several maxima, and occasionally the largest maximum did not correspond to the most likely choice for SS. We therefore developed a sliding window technique for computing correlation, and tossed out DTRs for which multiple maxima made the choice of phase ambiguous. Finally, we compared the SS-S residual determined by correlation with that deduced from an alternate technique, namely the autoregressional onset estimation algorithm of Pisarenko et al. [1987] which we used to estimate the onsets of the S and SS arrivals. This technique is particularly useful for quantifying the presence of a signal in a low S/N time series. A poor correspondence between the autoregressional and cross correlation techniques indicates an excess of noise, and we rejected observations for which these estimates differed by more than 5 s.

As a result of this filtering, we were left with 184 event-station pairs that we consider to be of acceptable quality. The standard deviation of the final data set containing 104 pairs of similar wavepaths is 1.6 s, which is similar to variations estimated by WM91. Our 56% rejection rate is much higher than the 13% of WM91, which we interpret as a testament to the generally better quality of digital data.

We then compared our observations with those previously reported by WM95 (Figure 4a). 97% of the DTRs in each data set are within a  $\pm 8$  s range have a mean near 0 s. DTRs are the same in most places where bounce points overlap. Both sets show coherent and large negative residuals in the western Himalaya and Pakistan (-3 to -8 s) and somewhat smaller negative residuals southwest of the Tibetan Plateau. Coherent positive residuals are observed beneath north-central Tibet, the Quaidam basin, the Qilian Shan range and the Tarim basin. At the same time, there are places where DTRs disagree. For example, we observe several small positive DTRs in central-southern Tibet, whereas those from WM95 are mostly negative. However, this

difference in residuals does not seem to be any more significant than the scatter in DTRs in each set, and we conclude that the data sets are reasonably compatible. Therefore, we merged our observations and interpret them together (Figure 4a).

While large-scale trends are evident in the map of individual measurements, coverage remains uneven and there is significant scatter in some areas. As discussed below, this scatter is most likely due to intrinsic uncertainties in the SS-S technique as opposed to an indication of any real structure beneath the bounce point. As very short wavelength patterns are unlikely to be significant, we smooth these patterns by calculating mean residuals in a  $2^{\circ} \times 2^{\circ}$  window that slides at  $1^{\circ}$  increments (Figure 4b).

The resulting pattern in Figure 4b summarizes our best estimate of SS-S DTRs for Tibet and surrounding regions. However, before we can interpret this picture in terms of upper mantle heterogeneity, we must account for the effects of crustal structure, local anisotropy, and global lateral heterogeneity.

#### *Effects of crustal structure and thickness*

Variations in crustal thickness in this region range from 30-40 km in low-lying areas to 60-70 km in the Tibetan Plateau and the surrounding mountains. Travel times for SS reflecting within the Tibetan Plateau (Figure 4) are thus delayed relative to those within (for example) India by excess crustal thickness. In order to account for variations in crustal thickness, crustal velocity structure, and topography, we calculated delay times using the GTOPO30 digital elevation model (REF) and the global crustal model CRUST5.1 [Mooney et al., 1998]. CRUST5.1 is based on seismic refraction data published between 1948-1995 and consists of  $5^{\circ}$  by  $5^{\circ}$  tiles in which the crust and uppermost mantle are described by eight layers. Average delays due to topography and excess crustal structure in the Tibetan Plateau are around 5 s (Figure 5a) for the angles of incidence of most of the SS paths in our data set. After this correction is applied (Figure 5b,c), DTRs everywhere become more negative, and the pattern is dominated by large negative residuals.

Of course, this correction is only as reliable as CRUST5.1. As a test of sensitivity we also estimated crustal corrections simply by using a crustal model derived from assuming isostatically compensated elevations and found that the patterns of corrections were not significantly different. Nevertheless, we note that recent studies suggest that the lower crust of Tibet has anomalously low wave speeds [e.g., Owens and Zandt, 1997; Nelson et al., 1996], which would

tend to increase the crustal delay and make the residual pattern even more negative, perhaps by an additional second.

#### *Effects of shear wave azimuthal anisotropy in the mantle*

Evidence has been accumulating over the past few years to suggest that the mantle beneath Eurasia is highly anisotropic. In fact, the strongest azimuthal anisotropy yet observed ( $\delta t = 2.4$ s) occurs in northeastern Tibet [McNamara et al., 1994], which means that an unfortunate combination of distant SS arrivals with the same bounce point but with azimuths differing by  $90^\circ$  could be offset by as much as 4.8 s. To estimate how significant this effect might be for our dataset, we use recent measurements of seismic anisotropy in the study region [Makeyeva et al., 1992; McNamara et al., 1994; Sandvol et al., 1994; Hirn et al., 1995; Sandvol et al., 1997; Guilbert et al., 1996] to develop an anisotropic correction map.

Because the measurements of anisotropy in Central Asia are still rather sparse, we have to make some gross assumptions in interpolating values of  $\delta t$  and  $\alpha$ . With few exceptions, the trend of fast axis  $\alpha$  in this area is nearly East-West, and so we assign an  $80^\circ$  fast axis direction to bounce points on the plateau and a  $110^\circ$  direction elsewhere. Delay times in the region vary from zero (no anisotropy detected) [Sandvol et al., 1994; Sandvol et al., 1997] in northern Pakistan to 2.4 s [McNamara et al., 1994] in northeastern Tibet. Nearly any interpolation scheme for  $\delta t$  will be speculative, so we simply assigned 0 s and 2.4 s to points that are near these extremes, and a “typical” value of 1 s elsewhere.

For this data set, most paths are oriented NW-SE and the maximum delays and advances are about 2 s. This kind of variation could explain some of the small-scale scatter observed both in this study and in prior shear-wave studies [e.g., Molnar, 1990, WM95]. One potentially can remove small-scale effects of anisotropy by averaging residuals with close bounce points and different azimuths. By the same token, an uneven distribution of event-station azimuths can introduce a systematic bias. Our modeling suggests that unaveraged anisotropy very likely contributes a regional bias on the order of  $\pm 1$  s.

#### *Effects of global scale laterally varying structure*

In order for SS-S DTRs to be interpreted in terms of structure beneath a bounce point, the total contribution to the travel time of shear wave speed heterogeneity outside of the source, receiver, and bounce point regions is presumed negligible. However, WM91 inferred that the

effects of the lower mantle can introduce variations on the order of 30%-40% of the total residuals, and Dricker and Roecker [1994] showed that in some cases large anomalies (as much as 8 s) can be caused by a combination of upper mantle heterogeneity and SS ray bending effects. Thanks to the efforts of global tomographers over the past decade, we should be able to estimate these effects not only statistically but also deterministically and calculate reasonable corrections to our travel times.

To estimate the effects of three-dimensional lateral variations in the Earth on our SS-S DTRs we trace rays through the global three-dimensional shear wave speed model of Grand et al. [1997; hereafter, G97]. Because SS is confined to the upper mantle over most of its journey from source to receiver, lateral heterogeneity can have a significant effect not only on travel time but also on the path of the wave through the Earth, and we attempted to estimate this effect by computation of actual ray paths. In practice we traced rays through 2D slices of the G97 model taken along the great circle path between source and receiver, mostly because the extra boundary conditions imposed by a floating bounce point on the Earth's surface makes true 3D tracing difficult. We note that tests in which we traced direct S waves in three dimensions suggest that the out-of-plane contribution to the travel time anomaly is relatively minor, typically differing from the 2D estimate by only a few tenths of a second. We employ an analytical ray tracing method described in detail elsewhere [Abers, 1992; Lin and Roecker, 1990], principally because the implementation of a reflection at the surface is straightforward. In two dimensions this technique is equivalent to that used in the Gaussian beam program Xgbm [Davis and Henson, 1993].

An unanticipated result of this exercise was the extent of multipathing produced by this relatively smooth model of the Earth; it is not unusual for 4-5 ray paths, with times as different as 10 seconds, to exist for a single source-receiver pair (Figure 6). Neglecting for the moment what this might imply for tomographic techniques that integrate travel times along 1D ray paths, we are faced with the question of how to decide which of these might be the phase corresponding to what we observe. We decided to select those paths that resulted in the minimum difference between observed and calculated DTRs. Often, but not always, this choice coincides with the minimum displacement of the bounce point from its 1D location. We note that the G97 model does a fairly decent job of explaining our SS-S DTRs, reducing the standard deviation of residuals from 4.8 s to 3.7 s.

Bounce points change location in the G97 model relative to the 1D model because of the loss of symmetry in upper mantle structure about the SS bounce point (Figure 6). The migration of bounce points appears chaotic in several regions, with displacements ranging from almost zero to several 100 km (Figure 7a). Nevertheless, the resulting smoothed image (Figure 8) looks not unlike that derived from 1D bounce points (Figure 5c), with at least one important exception: all of the points near (35°N, 82°E) that defined a zone of low wave speeds in north-central Tibet migrate northwards into the Tarim basin.

To the extent that the G97 model provides a reasonable representation of the Earth's mantle below depths of about 300 km, we can infer an upper mantle structure beneath the revised bounce points by differencing the observed SS-S from those calculated in the G97 model. The G97 model implicitly incorporates variations in crustal thickness, hence the same differencing corrects for the crustal contribution as well. The resulting residuals can then be used to deduce perturbations to wave speeds in G97 averaged over some depth range; we integrated through the mantle to 300 km as the contrasts above this depth in this model are on the order of  $\pm 3\%$ - $5\%$ , while those below are less than  $\pm 2\%$ . As discussed below, the resulting model (Figure 9b) shows much the same patterns as those inferred from G97 (Figure 9a), with highs and lows in the same geographic position and of similar wavelength, but with stronger contrasts.

To estimate the significance of using the G97 lower mantle as a proxy for that in the real Earth, we calculated the contributions along the ray paths below 300 km and determined a model of the upper mantle that would result if we made no correction for the lower mantle (i.e., we presume no unmodeled heterogeneity; this is equivalent to forcing all of the residual into the upper mantle). Contributions of the lower mantle are generally less than 4 s in magnitude but can be as high as 8 s (Figure 10). The effects on deduced upper mantle structure (Figure 9c) for most of the region are deviations in wave speed on the order of  $\pm 0.1$  km/s. The areas most influenced by these corrections are those to the north of the plateau, where wave speeds are systematically lower across a large area.

Clearly, an interpretation of SS-S residuals requires the determination of a number of corrections, but the uncertainties in any interpretation are a function of the uncertainties in the corrections, and not of the size of the corrections themselves. Based on the corrections we investigated, we conservatively estimate the overall uncertainty in the SS-S residuals to be about  $\pm 3$  s. Given that SS travel times in the upper mantle in the vicinity of the bounce point are about

100 s, this translates into a 3% uncertainty in inferred wave speed, or a variation of about  $\pm 0.14$  km/s.

### **Tectonic Implications**

The highest average wave speeds for the upper 300 km of the G97 model for the region of Tibet and surrounding areas (Figure 9a) appear in the west, beneath the Pamir, Karakorum, and western portion of the Tibetan plateau. Wave speeds are high as well to the south of Tibet, beneath Bangladesh and Burma, and east of the plateau beneath southern China. Wave speeds in the remainder of the Tibetan upper mantle generally are about 0.2 km/s higher than PREM, but the first order change from high to low wave speeds within Tibet appears as an east-west, rather than a north-south, variation.

The modification to the G97 model that we infer from SS-S DTRs preserves the patterns and wavelengths of these variations but enhances the contrasts. While the high wave speeds in the west remain at about the same level, this region is extended farther to the east, to about 88° E, and the wave speeds in the east generally become 0.2-0.3 km/s lower. Likewise, the low wave speeds to the north, under the Tarim Basin, decrease by 0.2-0.3 km/s and appear to be isolated from the plateau itself. Finally, the north-south band of lower wave speeds in far eastern Tibet, near 100° E, is enhanced by the SS-S perturbations.

Thus, while the SS-S model presented here supports a lateral variation in shear wave speeds across Tibet, the pattern appears to be dominated by an east-west gradient rather than a north-south one (Figure 9b). The existence of low wave speeds in the northeastern part of Tibet, east of about 88° E, has been reported in several high resolution studies [e.g., Wittlinger et al., 1996; McNamara et al., 1997; Kosarev et al., 1999], and these results corroborate the pattern we find here. Low wave speeds in the northern part of Tibet to the west of this longitude, which differ from what we report, have been inferred either from low resolution studies that include the eastern part of the plateau [e.g. Brandon and Romanowicz, 1986] or from other SS-S studies [WM95; Lyon-Caen, 1986]. We include the WM95 observations in this study; the difference in interpretation is a consequence of how corrections are applied and to the migration of bounce points associated with positive residuals outside of the plateau northwards into the Tarim basin as a result of ray tracing. We suggest that the very large delays reported by Lyon-Caen are to some extent caused by a combination of crustal delays and upper mantle anisotropy, the effects

of which are exacerbated by SS waves that spend a greater percentage of their time in the crust and upper mantle due to relatively short source-receiver distances (about 37 vs. the minimum 47 used here). For example, while the crustal corrections for the SS waves analyzed here are on the order of 5 s, the crustal correction for this shorter ray is about 9 s. Also, because this shorter-path SS wave traveled nearly parallel to the fast direction of anisotropy in Tibet, the effect of anisotropy is much more pronounced. When all of these corrections are accounted for (Table 1), the observed SS travel time appears to be within a second of the theoretically predicted value, whereas the observed travel time for the wave that bounced within the Indian Shield is faster than the theoretical travel time by about 5-6 s. Thus, it seems that this comparison of SS residuals does not demonstrate that wave speeds are slow beneath northern Tibet, but rather suggests that those beneath India are slightly faster than average.

The displacement of the slow bounce points into the Tarim Basin would suggest that the average wave speeds in the upper mantle beneath most of the basin are only slightly higher than those predicted by PREM, and the simplest interpretation would be that the lithosphere here is not significantly thicker, colder or stronger than average. However, in a study of surface waves traversing different parts of Asia, Curtis and Woodhouse [1997] inferred that the Tarim Basin has an unusually thick (53 km) and slow (2.8 km/s average) crust overlying an unusually fast (5.4 km/s) mantle lid between 53 km and 115 km depth. Nevertheless, the travel time of SS through their model is close to that predicted by PREM. In a sense, therefore, our results corroborate those of Curtis and Woodhouse [1997], and hence lend some support to geodynamical models of Asian evolution that postulate a strong lithosphere beneath the Tarim basin [e.g., England and Houseman, 1985]. We suggest, however, that higher resolution studies of this region are required to fully appreciate the role of this basin in Asian tectonics.

In general, our analysis of SS-S residuals indicates that, with the exception of a north-south oriented corridor in eastern Tibet, the upper mantle beneath Tibet is cold, and that the lithosphere is generally of normal to greater than normal thickness. These results therefore do not support the thin lithosphere models for the evolution of Tibet, which, by process of elimination, makes the thick lithosphere models more acceptable. Nevertheless, the dominant east-west gradients in wave speed imply that no two-dimensional model can satisfactorily explain the whole of Tibetan dynamics.

**Acknowledgements.** We would like to thank the operators of the seismic stations in the FSU for permission to use data from their archives. The cross correlation algorithm we used was adapted from one provided to us by Anne Sheehan and we appreciate her generosity. We thank Peter Molnar for the helpful comments. This -research was supported in part by NSF grant EAR-9219529.

### **References**

- Abers, G. A., 1992. Relationship between shallow- and intermediate-depth seismicity in the Eastern Aleutian subduction zone, *Geophys. Res. Let.*, 19, 2019-2023, 1992.
- Argand, E., La tectonique de l'Asie, *Proc. 13<sup>th</sup> Int. Geol. Congr.*, Brussels, 7, 171-372, 1924.
- Barazangi, M., and J. Ni, 1982. Velocities and propagation characteristics of Pn and Sn beneath the Himalayan arc and Tibetan plateau: Possible evidence for underthrusting of Indian continental lithosphere beneath Tibet. *Geology*, 10, 179-185.
- Brandon, C., and B. Romanowicz, A no-lid zone in the central Chang- Thang platform of Tibet, evidence from pure path phase-velocity measurements of long period Rayleigh-waves. *J. Geophys. Res.*, 91, 6547-6564, 1986.
- Choy, G. L., and P. G. Richards, Pulse distortion and Hilbert transformation in multiply reflected and refracted body waves, *Bull. Seismol. Soc. Am.*, 65, 55-70, 1975.
- Curtis, A., and J. Woodhouse, Crust and upper mantle shear velocity structure beneath the Tibetan plateau and surrounding regions from interevent surface wave phase velocity inversion, *J. Geophys. Res.*, 102, 11,789-11,813, 1997.
- Davis, J. P., and I. H. Henson, User's guide to Xgbm: an X-Windows system to compute Gaussian beam synthetic seismograms, Version 1.1, Teledyne Geotech Alexandria Laboratories publication TGAL-93-02, 1993.
- DeMets, C., Earthquake slip vectors and estimates of present-day plate motions, 98, 6703-6714, 1993.
- Dewey, J. F., and J. M. Bird, Mountain belts and the new global tectonics, *J. Geophys. Res.*, 75, 2625-2647, 1970.
- Dewey, J. F., and K. Burke, Tibetan, Variscan and Precambrian basement reactivation: products of a continental collision. *J. Geol.*, 81, 683-692, 1973.

- Dricker, I. G., and S. W. Roecker. Mapping of upper mantle shear wave velocity structure beneath Asia using SS-S data from Kirnos analog seismographs, EOS, Transaction, American Geophysical Union, 75, 464, 1994.
- Dricker, I. G., L. P. Vinnik, S. W. Roecker, L. I. Makeyeva, Upper-mantle flow in Eastern Europe, Geophys. Res. Lett., 26, 1219-1222, 1999.
- Dziewonski, A. M., and D. L. Anderson, Preliminary reference earth model, Phys. Earth Planet. Inter., 25, 297-356, 1981.
- Dziewonski, A. M., and F. Gilbert, The effect of small, aspherical perturbations on travel times and a re-examination of the corrections for ellipticity, Geophys. J. R. Astron. Soc., 44, 7-17, 1976.
- England, P., and G. Houseman, Role of lithospheric strength heterogeneities in the tectonics of Tibet and neighbouring regions, Nature, 315, 297-301, 1985.
- Fisher, R. L., J. G. Sclater, and D. P. McKenzie, Evolution of the Central Indian ridge, western Indian ocean, Geol. Soc. Am. Bull., 82, 553-562, 1971.
- Grand, S. P., and D. V. Helmberger, Upper-mantle shear structure beneath Asia from multi-bounce S-waves, Phys. Earth Planet. Inter., 41, 154-169, 1985.
- Grand, S. P., R. D. van der Hilst, R. D., and S. Widiyantoro, Global seismic tomography; a snapshot of convection in the Earth, GSA Today, 7, 1-7, 1997.
- Guilbert, J.; Poupinet, and G.; Jiang Mei, A study of azimuthal P residuals and shear-wave splitting across the Kunlun Range (northern Tibetan Plateau), Phys. Earth Planet. Inter., 95, 167-174, 1996.
- Hirn, A., M. Jiang, M. Sapin, J. Diaz, A. Nercessian, Q. Lu, J. C. Lepine, D. N. Shi, M. Sachpazi, M. R. Pandey, K. Ma, and J. Gallart, Seismic anisotropy as an indicator of mantle flow beneath the Himalayas and Tibet, Nature, 375, 571-574, 1995.
- Holt W.E., and T. C. Wallace, Crustal thickness and upper mantle velocities in the Tibetan Plateau region from the inversion of regional Pnl waveforms: evidence for a thick upper mantle lid beneath southern Tibet, J. Geophys. Res., 95, 12, 499-12, 526, 1990.
- Houseman, G. A., D. P. McKenzie, and P. Molnar, Convective instability of a thickened boundary layer and its relevance for the thermal evolution of continental convergent belts, J. Geophys. Res., 86, 6115-6132, 1981.

- Kosarev, G. L., N. V. Petersen, L. P. Vinnik, and S. W. Roecker, Receiver function for the Tien Shan analog broadband network: Contrast in the evolution of structure across the Talasso-Fergana fault, *J. Geophys. Res.*, 98, 4437-4448, 1993.
- Kosarev G., R. Kind, S. V. Sobolev, X. Yuan, W. Hanka, S. Oreshin, Seismic evidence for a detached Indian lithospheric mantle beneath Tibet, *Science*, 283, 1306-1309, 1999.
- Lin, C.-H., and S. W. Roecker, Determination of earthquake hypocenters, focal mechanisms, and velocity structures in the Morgan Hill area through 3-D circular ray tracing, *EOS Trans. AGU*, 81, 1445, 1990.
- Lyon-Caen H., Comparison of the upper mantle shear wave velocity structure of the Indian Shield and the Tibetan Plateau and tectonic implications, *Geophys. J. R. Astron. Soc.*, 86, 727-749, 1986.
- Makeyeva, L.I., L. P. Vinnik, and S. W. Roecker, Shear-wave splitting and small-scale convection in the continental upper mantle, *Nature*, 358, 144-147, 1992.
- McNamara, D. E., T. J. Owens, P. G. Silver, and F. T. Wu, Shear wave anisotropy beneath the Tibetan Plateau, *J. Geophysics. Res.*, 89, 13,655-13,666, 1994.
- McNamara, D. E., T. J. Owens, and W. R. Walter, Upper mantle velocity structure beneath the Tibetan Plateau from Pn travel time tomography, *J. Geophys. Res.*, 102, 493-505, 1997.
- Molnar, P., and P. Tapponier, Cenozoic tectonics of Asia: Effects of continental collision, *Science*, 189, 421-426, 1975.
- Molnar, P., and P. Tapponier, Relation of eastern China to the India-Eurasia collision: application of slip-line field theory to large-scale continental tectonics, *Geology*, 5, 212-216, 1977.
- Molnar, P., and W. P. Chen, S-P-wave traveltimes residuals and lateral inhomogeneity in the mantle beneath Tibet and the Himalaya, *J. Geophys. Res.*, 89, 6911-6917, 1984.
- Molnar, P., S-wave residuals from earthquakes in the Tibetan region and lateral variations in the upper mantle, *Earth Planet. Sci. Lett.*, 101, 68-77, 1990.
- Mooney, W. D., G. Laske, and T. G. Masters, CRUST 5.1; a global crustal model at 5 degrees X5 degrees. *J. Geophys. Res.*, 103, 727-747, 1998.
- Nelson, K. D., W. Zhao, L. D. Brown, J. Kuo, J. Che, X. Liu, S. L. Klemperer, Y. Makovsky, R. Meissner, J. Mechie, R. Kind, F. Wenzel, J. Ni, J. Nabelek, C. Leshou, H. Tan, W. Wei, A. G. Jones, J. Booker, M. Unsworth, W. S. F. Kidd, M. Hauck, D. Alsdorf, A. Ross, M. Cogan,

- C. Wu, E. Sandvol, and M. Edwards, Partially molten middle crust beneath southern Tibet: Synthesis of project INDEPTH results. *Science*, 274, 1684-1688, 1996.
- Ni, J. and M. Barazangi, High-frequency seismic-wave propagation beneath the Indian shield, Himalayan arc, Tibetan Plateau and surrounding regions – high uppermost mantle velocities and efficient Sn propagation beneath Tibet. *J. Geophys. Res.*, 72, 665-689, 1983.
- Owens T., and G. Zandt, Implications of crustal property variations for models of Tibetan plateau evolution. *Nature*, 387, 37-43, 1997.
- Pandey, M. R., S. W. Roecker, and P. Molnar, P-wave residuals at stations in Nepal: evidence for a high velocity region beneath the Karakorum. *Geophys. Res. Lett.*, 18, 1909-1912, 1991.
- Patriat, P., and J. Achache, India-Asia collision chronology and its implication for crustal shortening and driving mechanisms of plates, *Nature*, 311, 615-621, 1984.
- Pisarenko, V. F., A. F. Kushnir, and I. V. Savin, Statistical adaptive algorithms for estimation of onset moments of seismic phase, *Phys. Earth Plan. Int.*, 47, 4-10, 1987.
- Romanowicz, B., Constraints on the structure of the Tibetan Plateau from pure path phase velocities of Love and Rayleigh-waves, *J. Geophys. Res.*, 87, 6865-6883, 1982.
- Sandvol, E A; Ni, J F; Hearn, T M; and Roecker, S., Seismic Azimuthal Anisotropy Beneath The Pakistan Himalayas, *Geophys. Res. Let*, 21, 1635-1638, 1994.
- Sandvol, E., J. Ni, R. Kind, and W. Zhao, Seismic anisotropy beneath the southern Himalayas-Tibet collision zone. *J. Geophys. Res.*, 102, 17,813-17,823, 1997.
- Searle, M. P., et al., The closing of Tethys and the tectonics of the Himalaya, *Geol. Soc. Am. Bull*, 98, 678-701, 1987.
- Sheehan A. F., and S. C. Solomon, Joint inversion of shear wave travel time residuals and geoid and depth anomalies for long-wavelength variations in upper mantle temperature and composition along the mid-Atlantic ridge, *J. Geophys. Res.*, 96, 19,981- 20,009, 1991.
- Tapponnier, P., G. Peltzer, A. Y. Ledain, R. Armijo, and P. Cobbold, Propagating extrusion tectonics in Asia: new insight from simple experiments with plasticine, *Geology*, 10, 611-616, 1982.
- Usenko A. Yu., Azimuthal anisotropy of lithosphere in the territory of the USSR (in Russian), Ph.D. thesis, Inst. Phys. of the Earth, Moscow, 145 pp., 1991.
- Vinnik, L.P., Makeyeva, L.I., Miley, and A., Usenko, A. Yu., Global pattern of azimuthal anisotropy and deformations in the continental mantle. *Geophys. J. Int.*, 111, 433-447, 1992.

- Willet S. D., C. Beaumont, Subduction of Asian lithospheric mantle beneath Tibet inferred from models of continental collision, *Nature*, 369, 642-645, 1994
- Wittlinger, G., F. Masson, G. Poupinet, P. Tapponnier, J. Mei, G. Herquel, J. Guilbert, U. Achauer, X. Guanqi, and S. Danian, Lithoscope Kunlun Team, Seismic tomography of Northern Tibet and Kunlun: Evidence for crustal blocks and mantle velocity contrasts. *Earth Planet. Sci. Lett.*, 139, 263-279, 1996.
- Woodward, R. L., and G. Masters, Global upper mantle structure from long-period differential travel times, *J. Geophys. Res.*, 96, 6351-6377, 1991.
- Woodward, R. L., and P. Molnar, Lateral heterogeneity in the upper mantle and SS - S traveltime intervals for SS rays reflected from the Tibetan Plateau and its surroundings, *Earth and Planet. Sci. Lett.*, 135, 139-148, 1995.
- Zhoa, L., and J. Xie, Lateral variation in compressional velocities beneath the Tibetan Plateau from Pn travel-time tomography, *Geophys. J. Int.*, 115, 1070-1084, 1993.
- Zhao, L.-S., M. K. Sen, P. Stoffa, and C. Frohlich, Application of very fast simulated annealing to the determination of the crustal structure beneath Tibet. *Geophys. J. Int.*, 125, 355-347, 1996.
- Zhao, W. and J. Morgan, Uplift of the Tibetan Plateau, *Tectonics*, 4, 359-369, 1985.

## FIGURE CAPTIONS

Figure 1. Topographic map of the Tibetan Plateau and surrounding regions. Solid lines show major faults (ATF – Altyn Tagh Fault; NKF – North Kunlun Fault; KTF – Kang Ting Fault; MCT – Main Central Thrust; MBT – Main Boundary Thrust) and dashed lines indicate suture zones that bound tectonic terrains of the plateau (JRS – Jinsa River Suture; BNS – Banggong Nujiang Suture; ITS – Indus-Tsangpo Suture).

Figure 2. Cartoons summarizing current two-dimensional models of the dynamics of the Tibetan Plateau. (A) Underthrusting of the Indian lithosphere [Argand, 1924; Ni and Barazangi, 1983] beneath the Tibetan Plateau; (B) a variation of the underthrusting model in which the Indian lithosphere continues to subduct, but the crust is injected into the lower crust beneath the Tibetan Plateau [Zhao and Morgan, 1985]; (C)

distributed thickening of the Asian lithosphere by an indentation of the stronger Indian lithosphere [Dewey and Bird, 1970; Dewey and Burke, 1973]; (D) a modification of the underthrusting model [Owens and Zandt, 1997], in which the lithosphere is practically absent beneath central Tibetan Plateau bounded by Bangong suture to the South and Qaidam basin to the North (a model by Kosarev et al., [1999] is similar to this model, but there the subducting Indian lithosphere is detached and extends to a depth of 200 km beneath the Bangong suture); (E) a low velocity zone in the mantle of the northern Tibet explained by the retreat of the Asian lithosphere [Willett and Beaumont, 1994]; (F) a modification of model (E) which includes a convective removal of the thickened Asian lithosphere [Houseman et al., 1981].

Figure 3. Location of events (circles), stations (triangles) and 1D bounce points ( crosses) for the 421 new SS observations collected from the archives of analog stations in the former Soviet Union.

Figure 4. (a) Differential travel time residuals ( $[\text{SS-S}]_{\text{observed}} - [\text{SS-S}]_{\text{PREM}}$ ) for the 184 selected arrivals from this study ( white symbols, black background) combined with those reported by Woodward and Molnar [1995] ( black symbols, white background). The meaning of the symbols is the same as in Figure 5.

Negative residuals are triangles and positive residuals are squares, with size corresponding to residual magnitude as shown in the scale at the bottom of the figure. The orientations (azimuths) of the great-circle ray paths are shown by the lines emanating from the symbols. (b) Spatially averaged DTRs for a combination of both data sets.

Figure 5. (a) A map of CRUST5.1 and topographic corrections (in seconds for a one-way traveltime) for the DTRs observed in this study and those reported by Woodward and Molnar [1995]. (b) Individual differential travel time residuals ( $[\text{SS-S}]_{\text{observed}} - [\text{SS-S}]_{\text{PREM}}$ ) after the crustal and topographic correction. (c) Spatially averaged residuals.

Figure 6. An example of ray tracing S and SS ray paths in the G97 model. Shown is a great circle cross-section of the G97 model between the source, located at (5.14°N, 127.41°E) and 114 km depth, and the receiver at (42.7°N, 73.8°E). The extremes of wave speed perturbation shown in the color bar are chosen to accentuate variations

in the lower mantle; perturbations in the upper 300 km can be as large as  $\pm 5\%$ . S and SS rays traced through a one-dimensional Earth are shown as green lines; those traced through the G97 section are shown as black lines. Note that the S ray paths are nearly identical in the 3D and 1D models, but the SS ray paths are different and are subject to multipathing effects. The S travel time is about 2.8 s faster in the G97 model than in the 1D model. With increasing distance from the source (left edge of figure) to the bounce points, SS times are 1.3 s slower, 4.8 s faster, and 3.8 s faster than the 1D time. The difference between observed SS-S and that calculated for the G97 model is nearly zero for the bounce point farthest from the source.

Figure 7. Results of ray tracing through the G97 model. (a)  $[SS-S]_{G97} - [SS-S]_{PREM}$  DTRs plotted at 3D bounce points, with locations of 1D bounce points shown by the line emanating from each symbol. (b) Smoothed version of the residuals shown in (a).

Figure 8. Results of ray tracing through the G97 model. Smoothed  $[SS-S]_{observed} - [SS-S]_{G97}$  DTRs mapped at the 3D bounce points. To the extent that the G97 model accurately models the crust and topography of Central Asia and the lower mantle of the Earth, these residuals reflect deviations to the G97 model of the upper mantle in the vicinity of the bounce points.

Figure 9. (a) Average wave speeds in the upper 300 km of the G97 model of the mantle (crustal contributions removed). (b) Modifications of (a) required to explain the smoothed residuals shown in Figure 8. (c) Modifications of (a) required if no corrections are made for the contribution of the lower mantle. Wave speeds are indicated at the bottom of the figure. The average value for PREM is indicated on the color bar. White boxes correspond to regions with no new information.

Figure 10. Contribution to SS-S residuals by lower mantle heterogeneity in the G97 model. Magnitude is given by the color bar to the right.

Table 1. A comparison of the SS travel times for the events from the study of Lyon-Caen [1986].

Event	Jan. 10, 1979	Dec. 15, 1982
Station	KMI	WHN
Ray path	Indian shield	Northern Tibet
Distance	37.5 <sup>0</sup>	37.9 <sup>0</sup>
Observed SS-S	160	185
Correction for crustal	0	9

thickness		
Correction for elevation	0	4
Anisotropy correction	0	4
Corrected SS-S	160	168
IASP91 S	783.47	789.53
IASP 91 SS	948.95	957.05
IASP 91 SS-S	165.48	167.52
Observed-IASP91	-5.5 s	-0.5 s

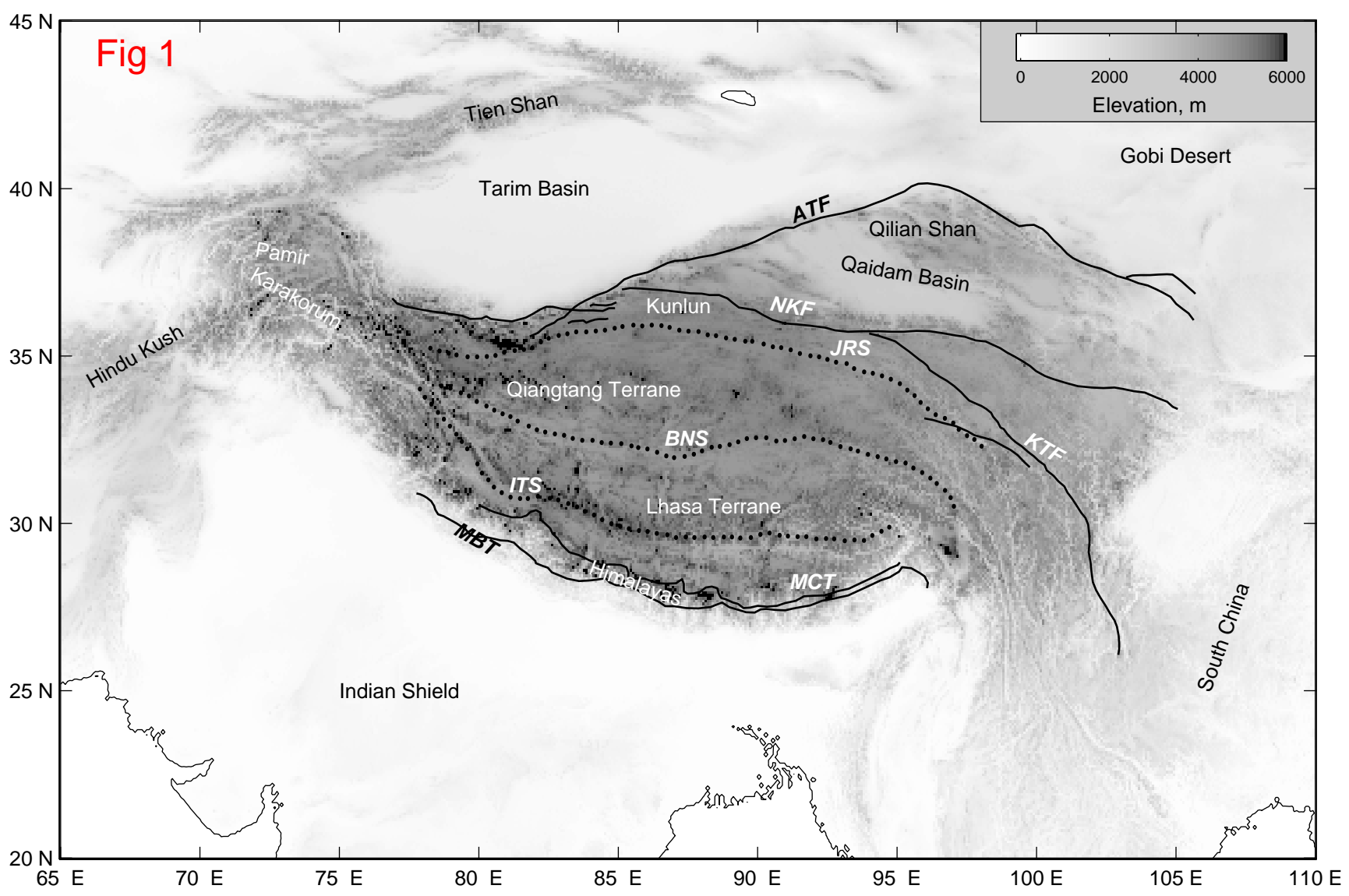
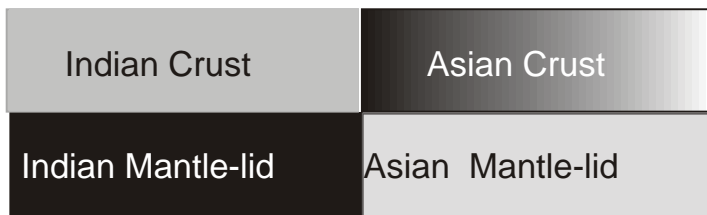
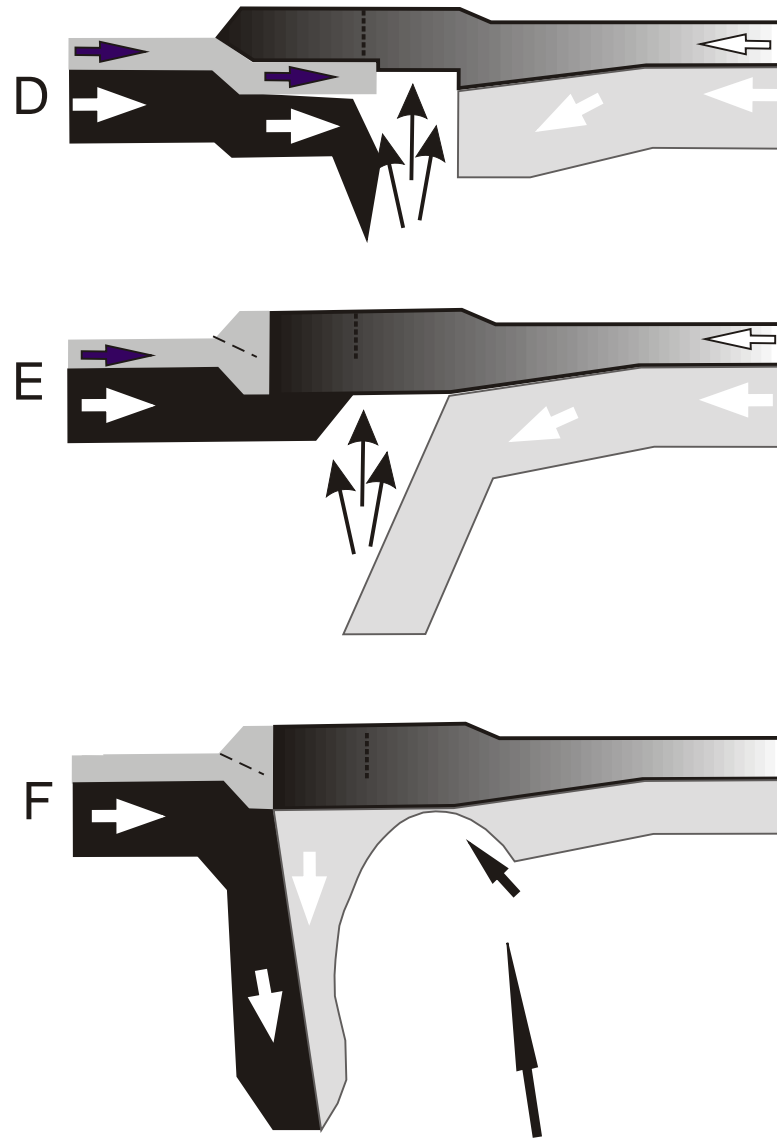
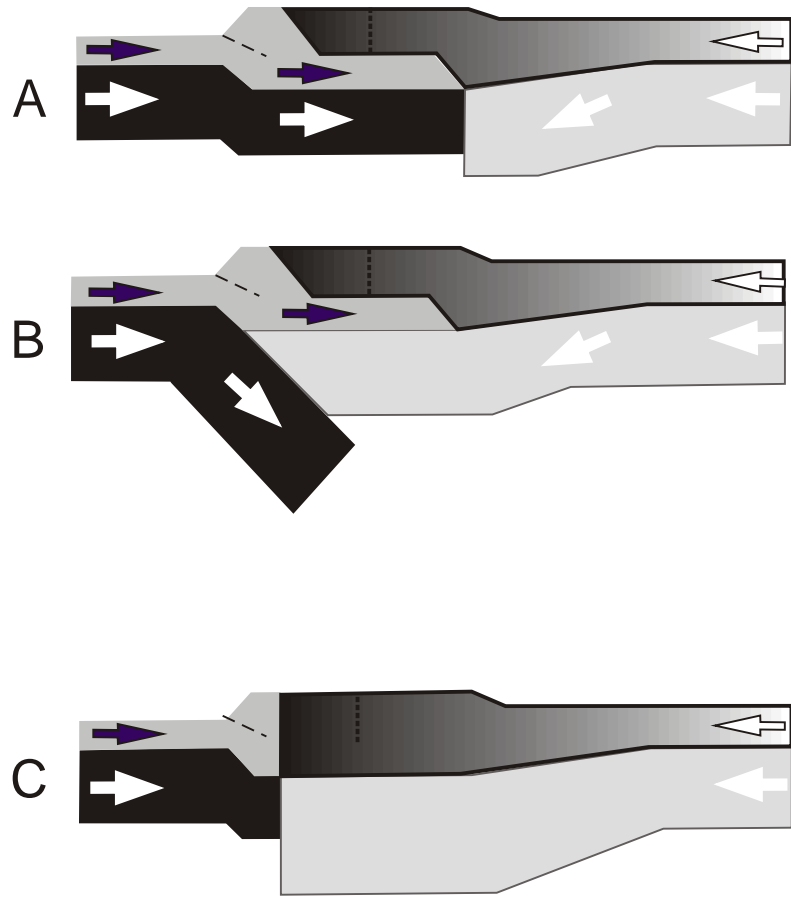


Fig. 2



Asthenosphere

Fig. 3

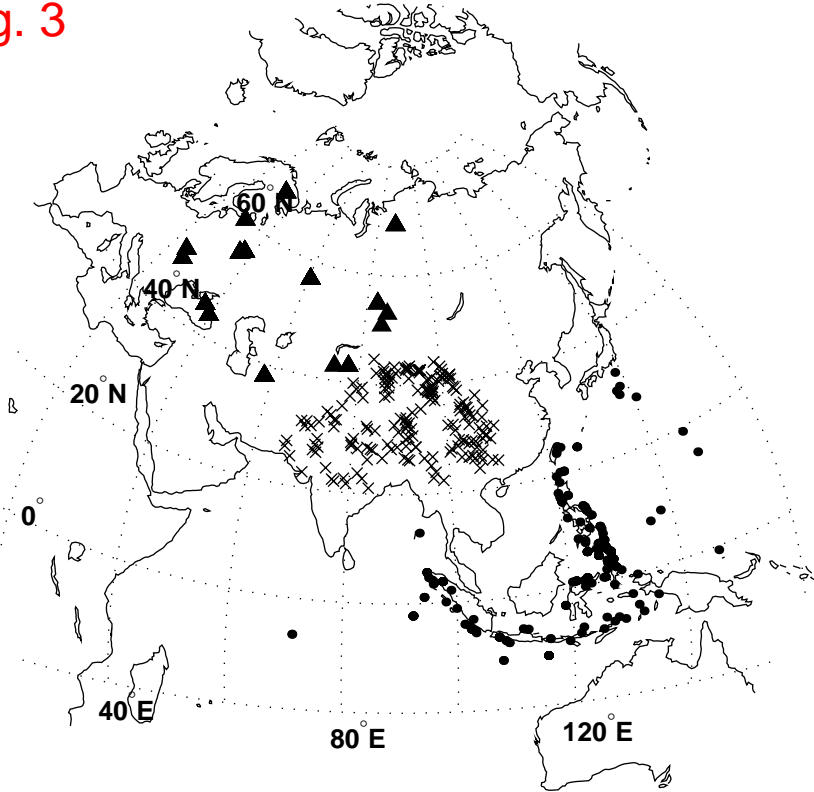


Fig. 4a

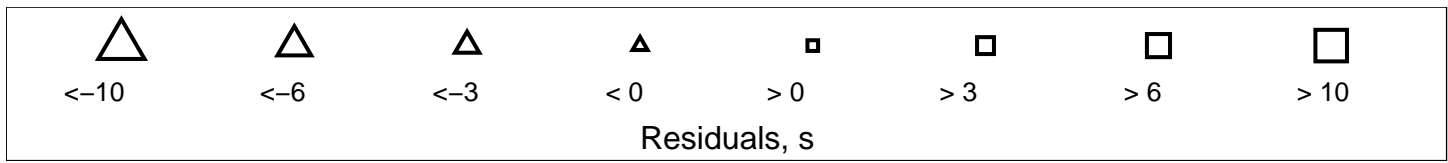
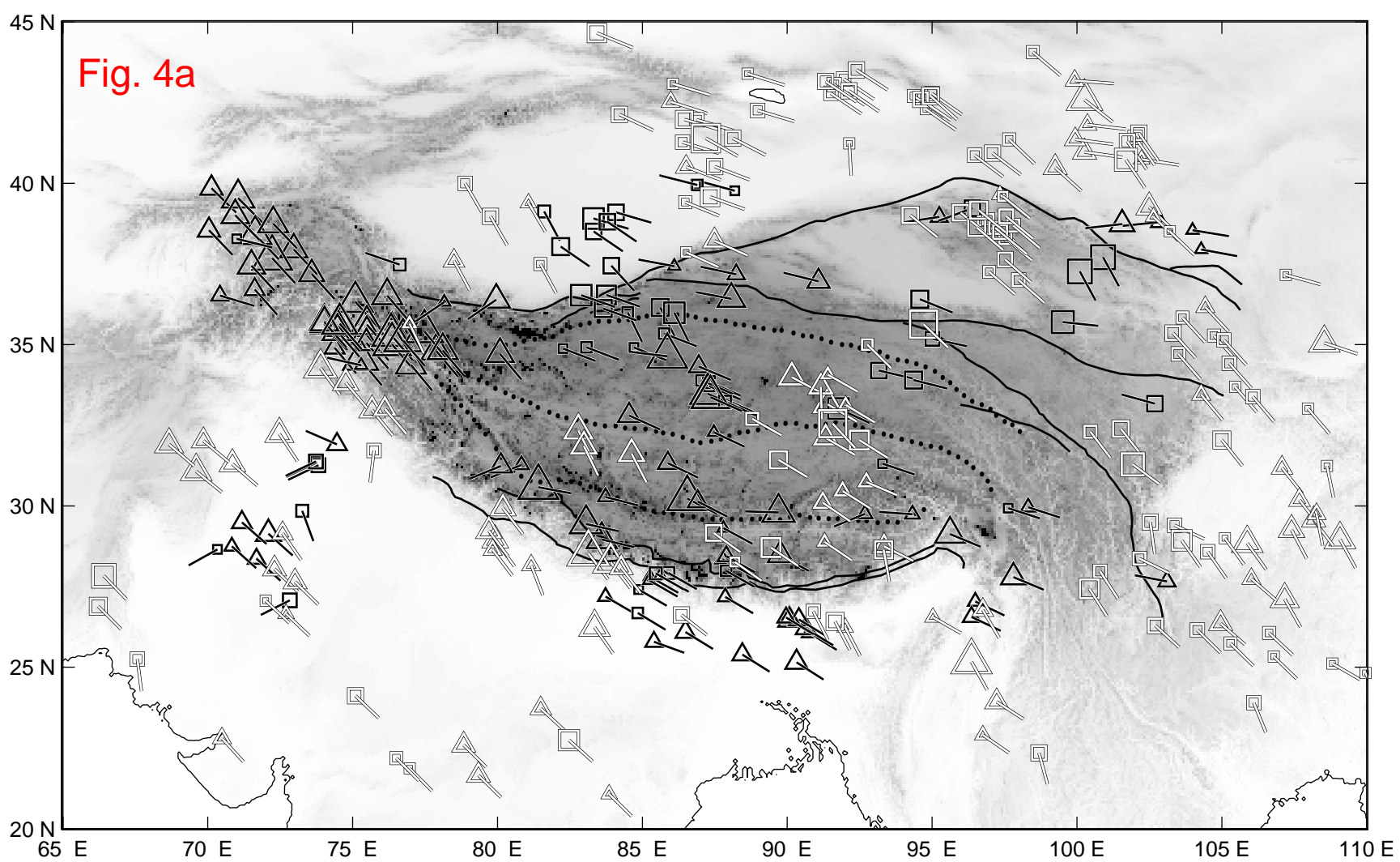


Fig. 4b

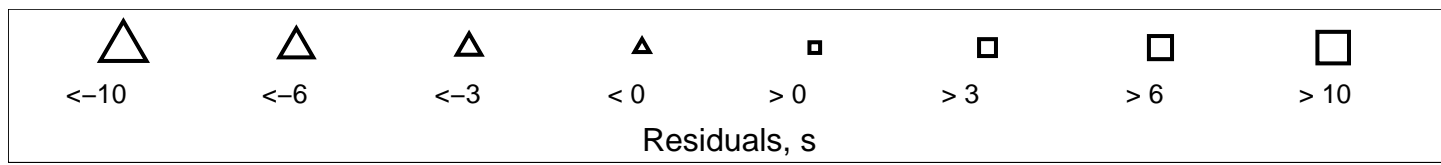
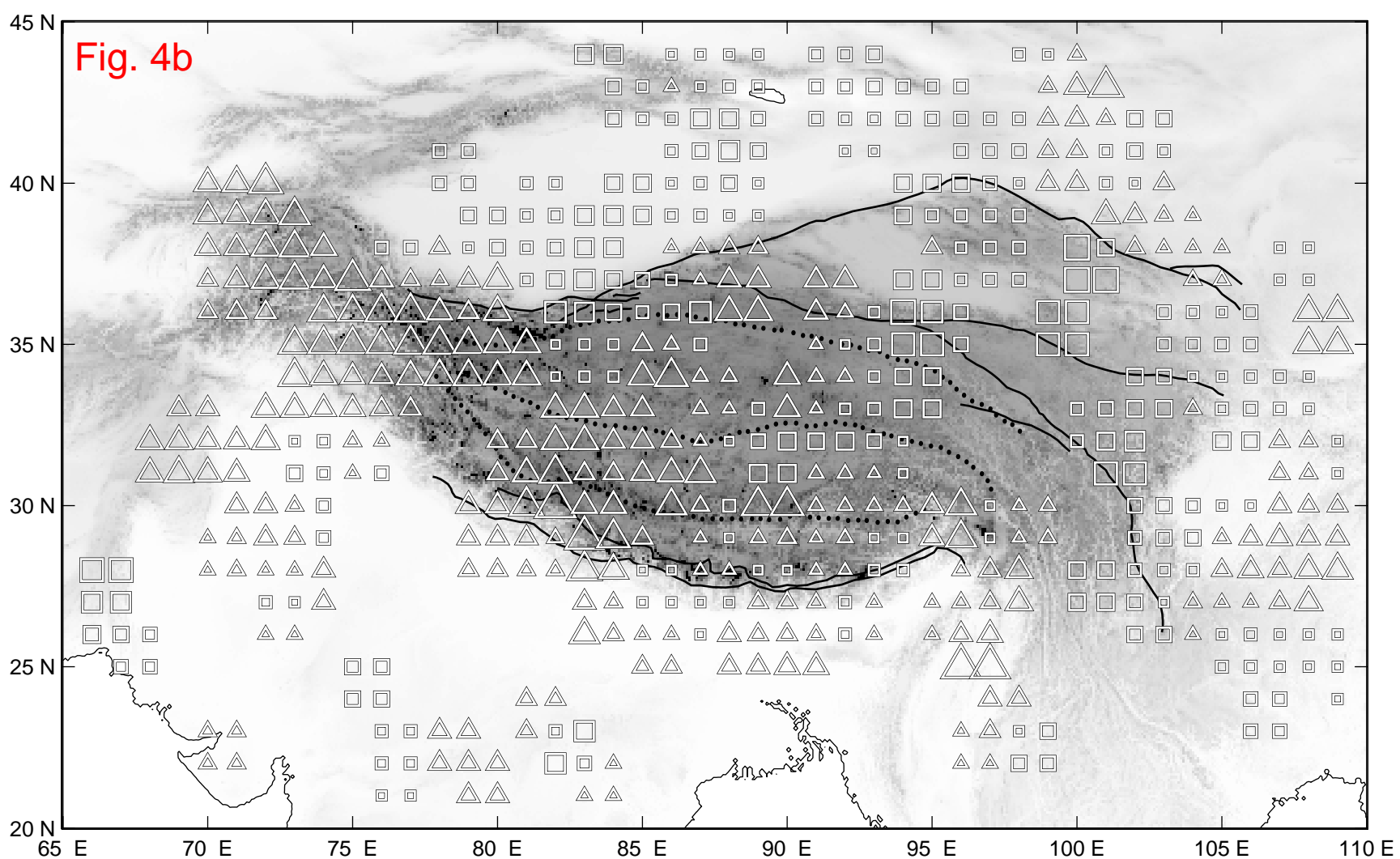


Fig. 5a

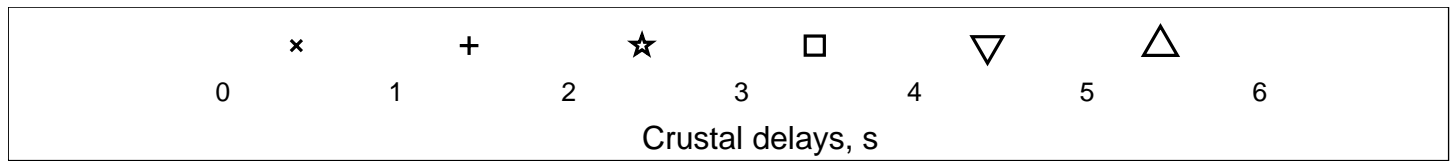
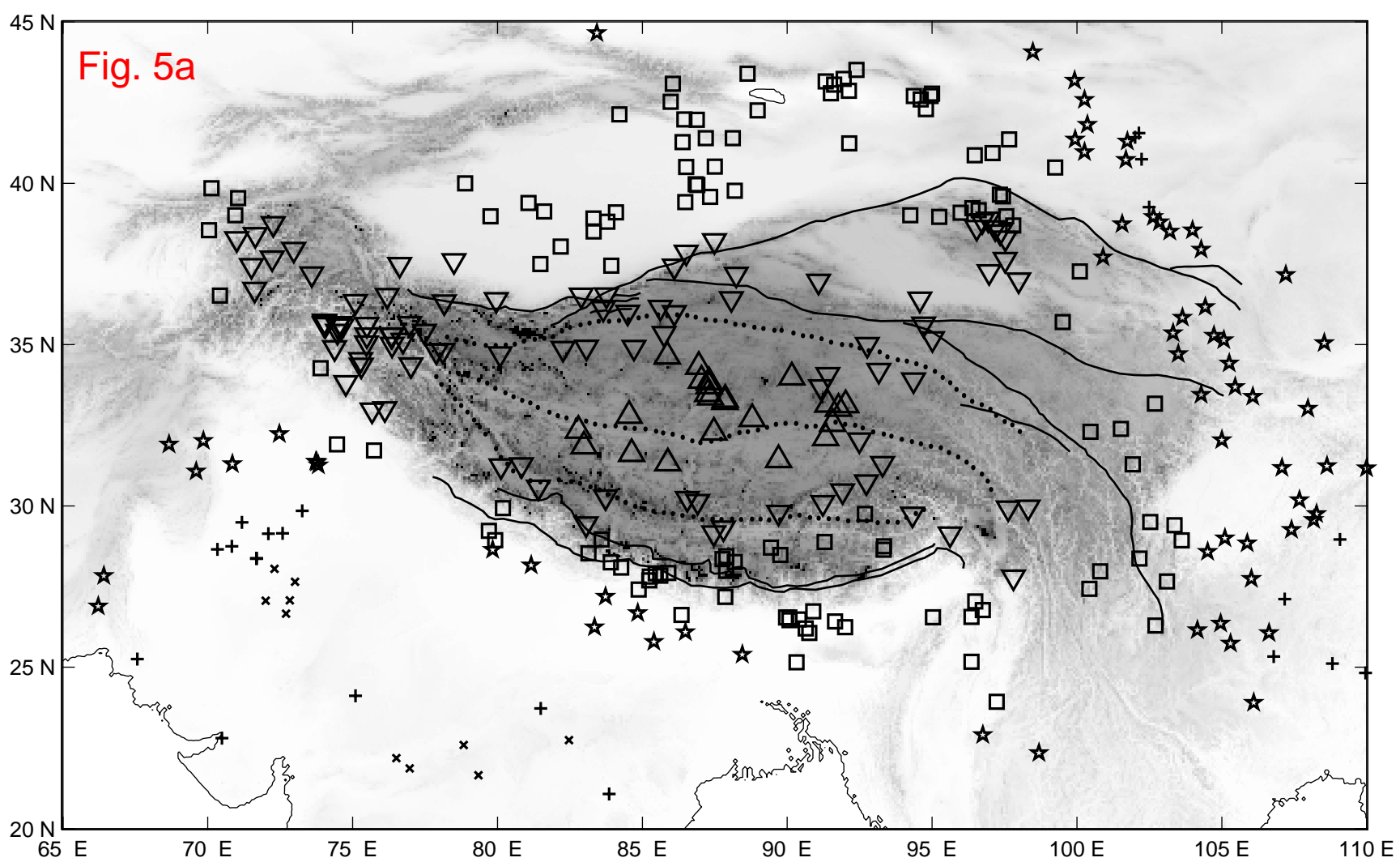


Fig. 5b

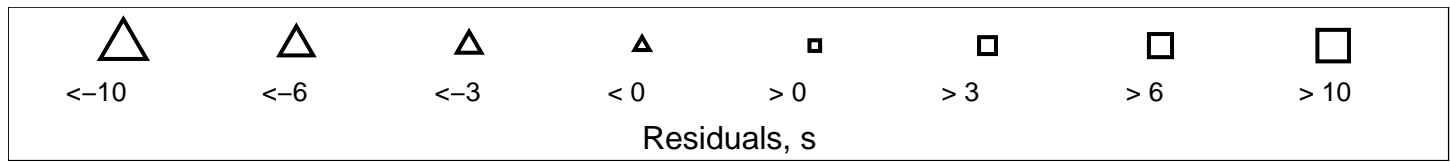
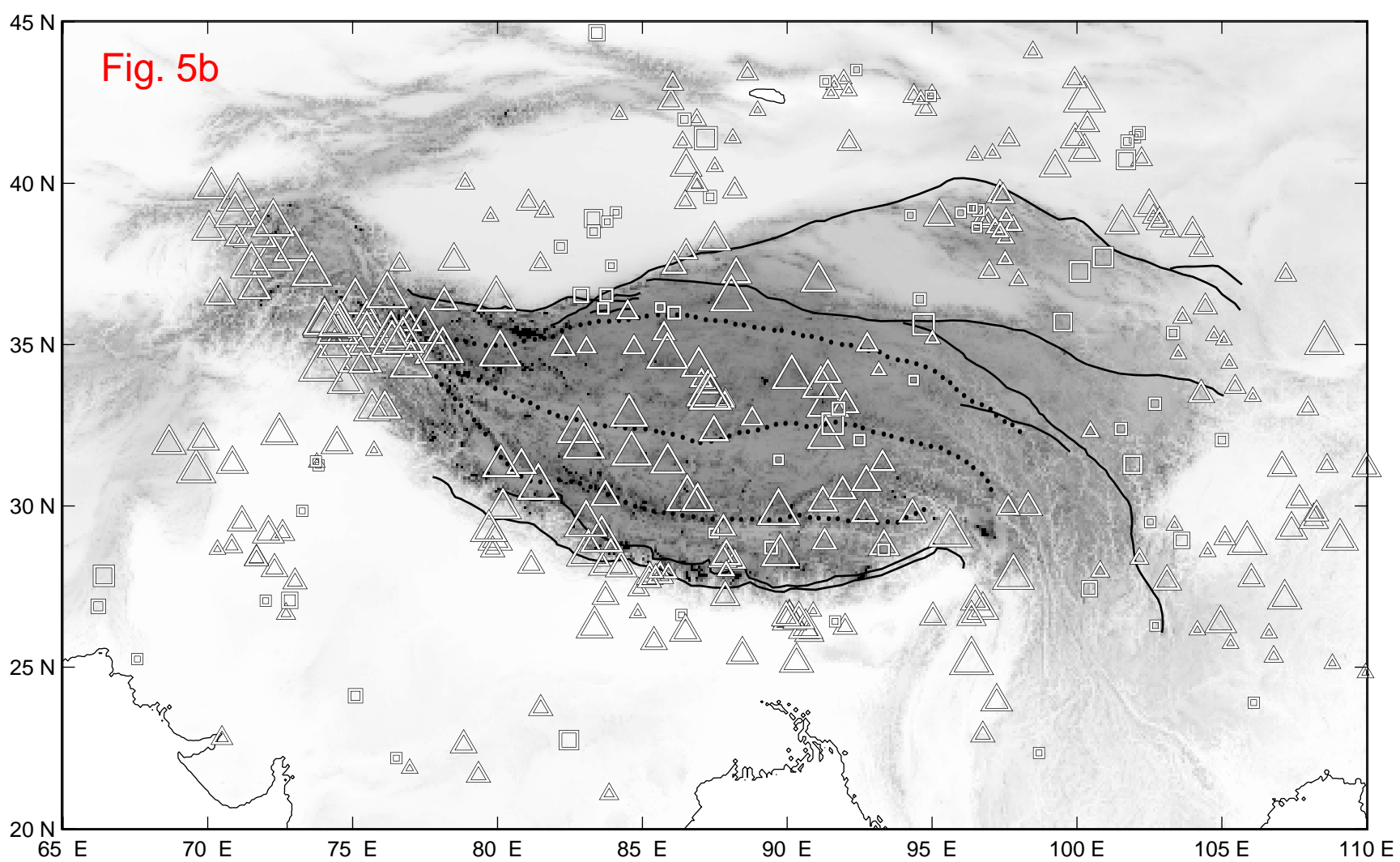


Fig. 5c

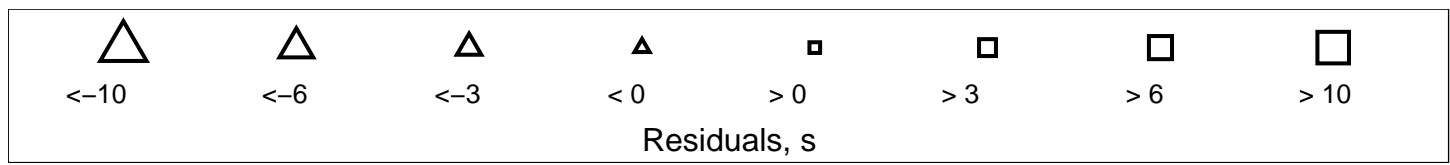
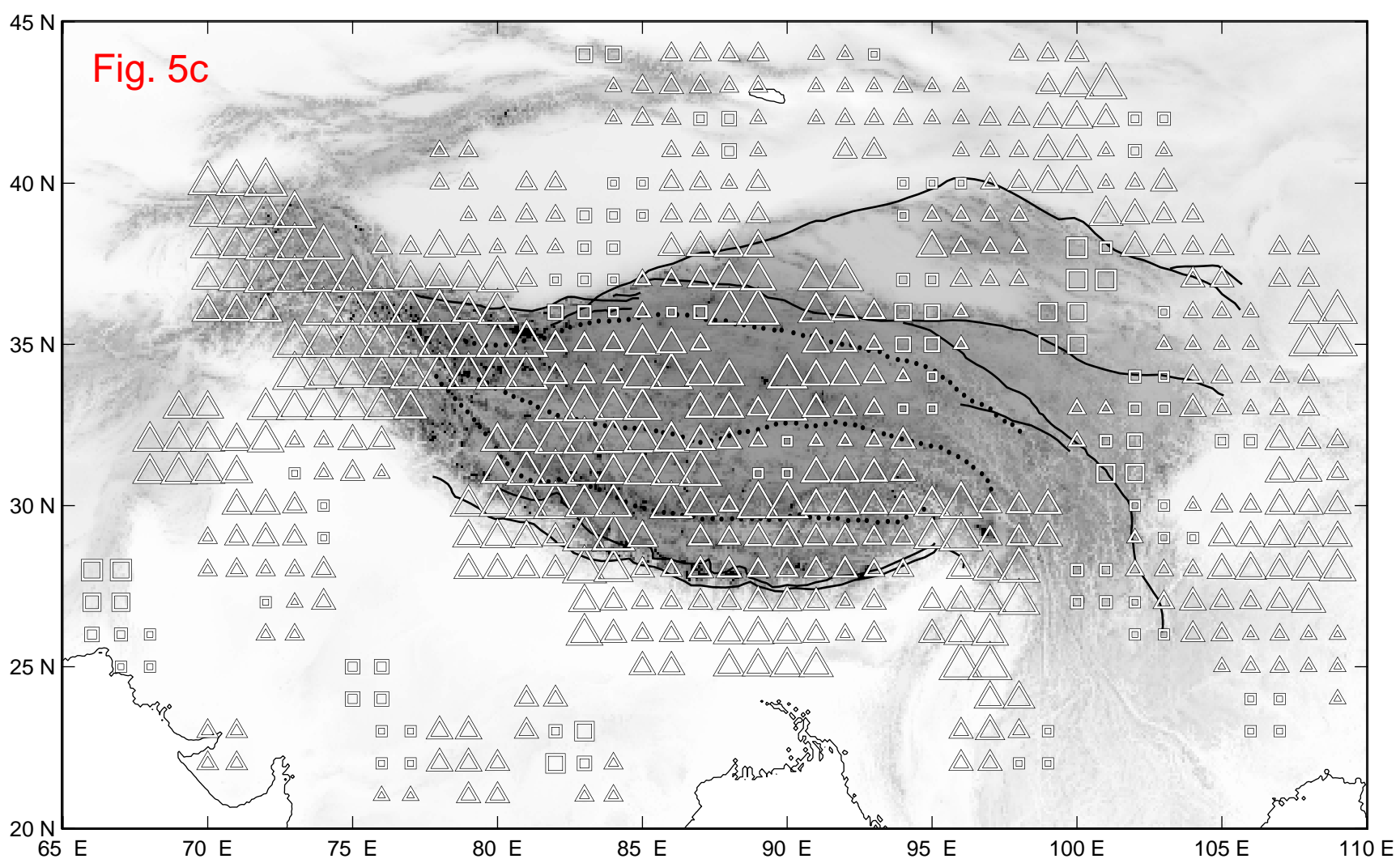


Fig. 6

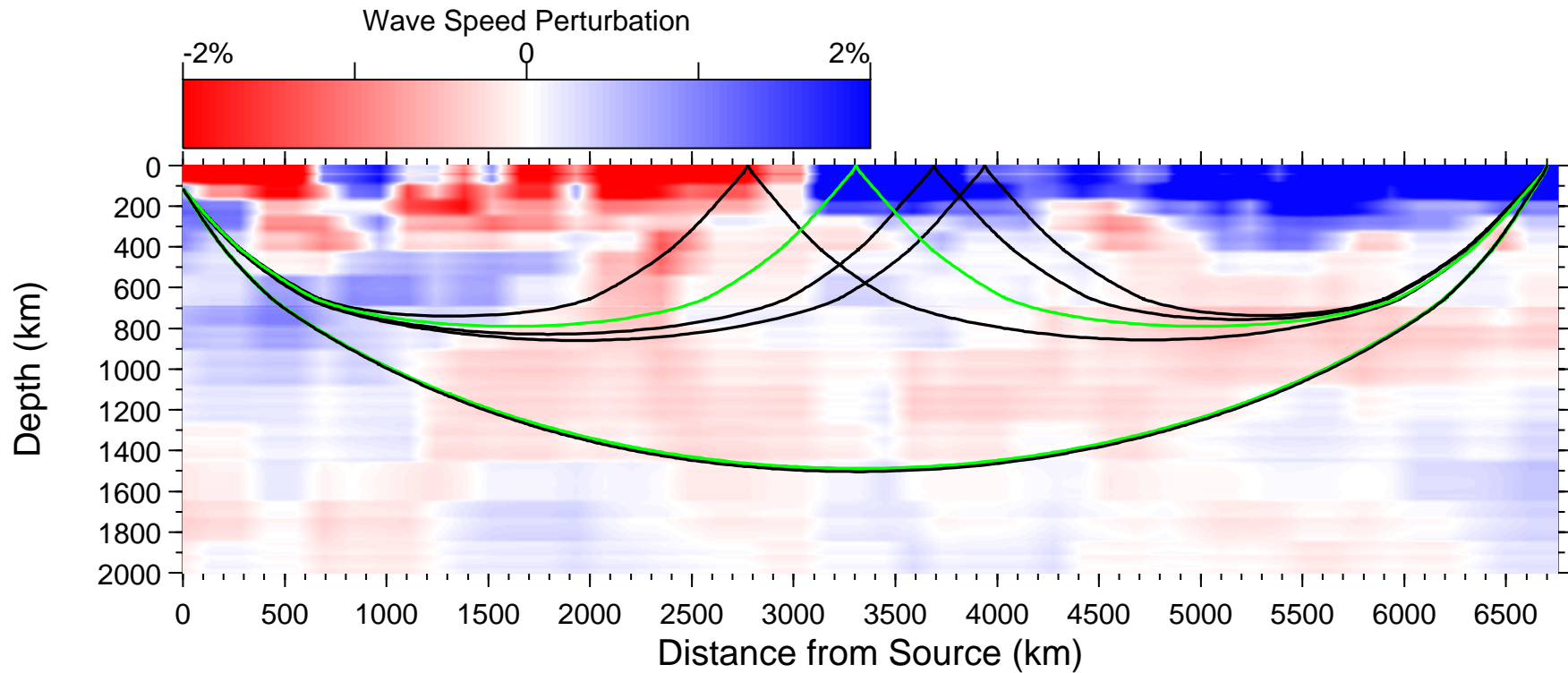


Fig 7a

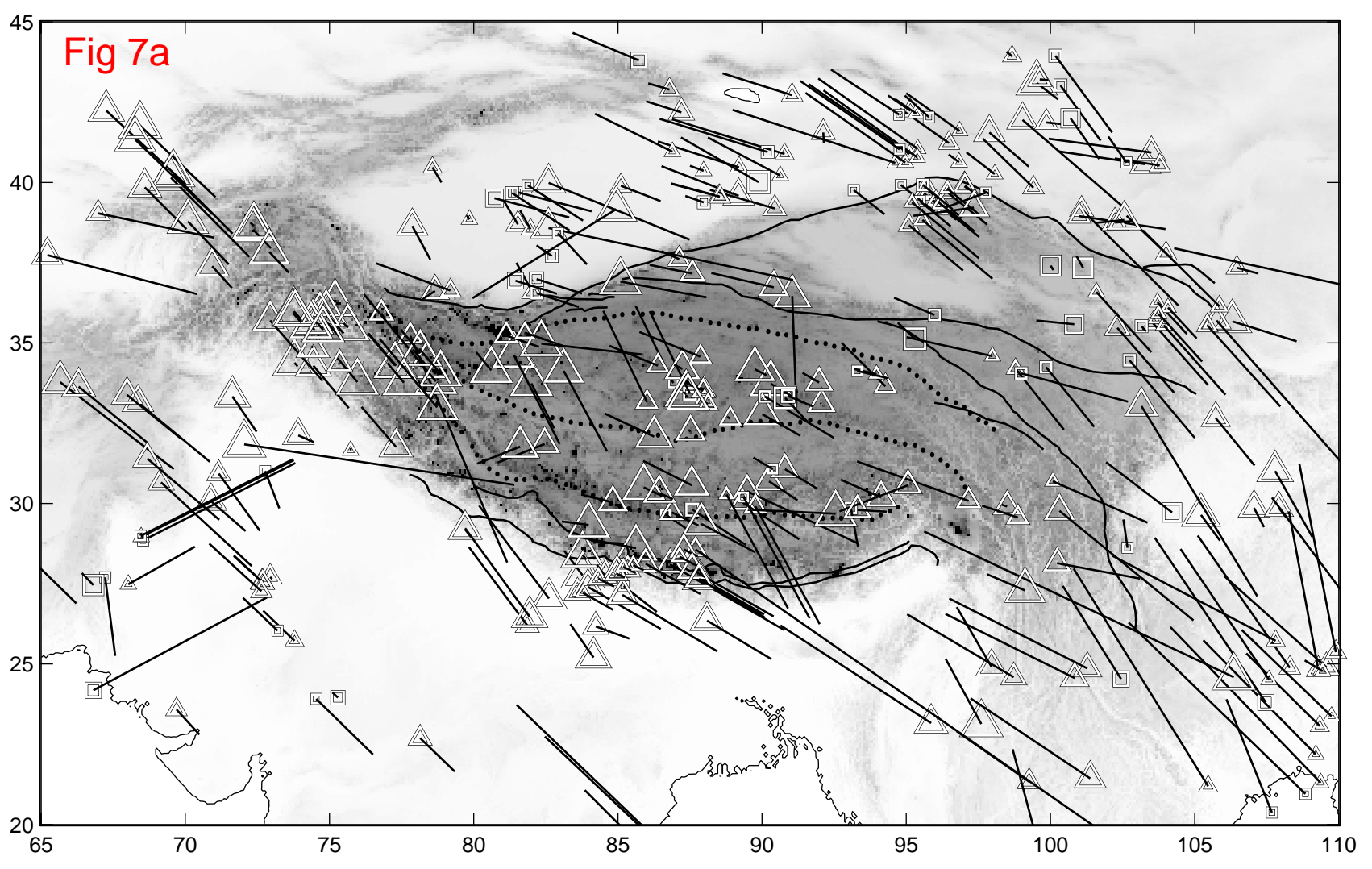


Fig. 7b

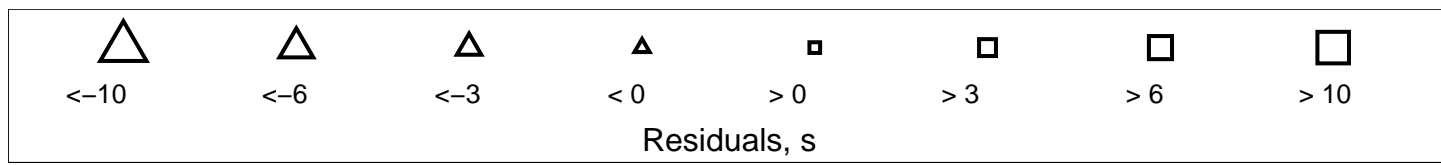
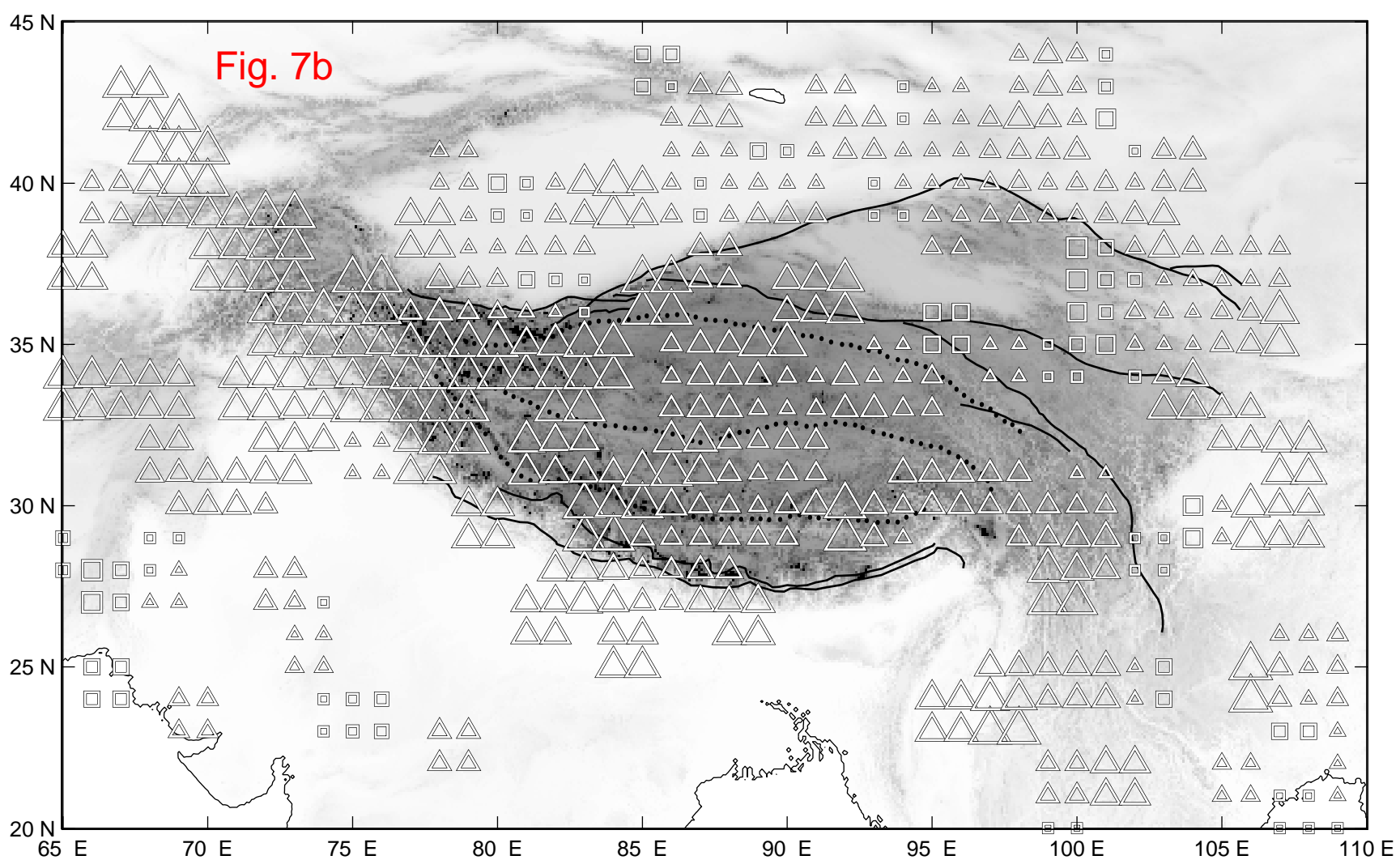


Fig. 8

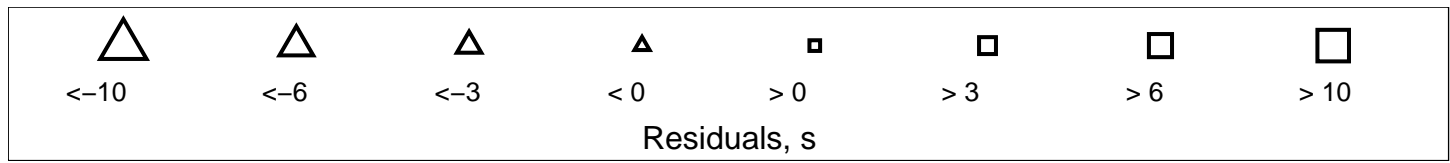
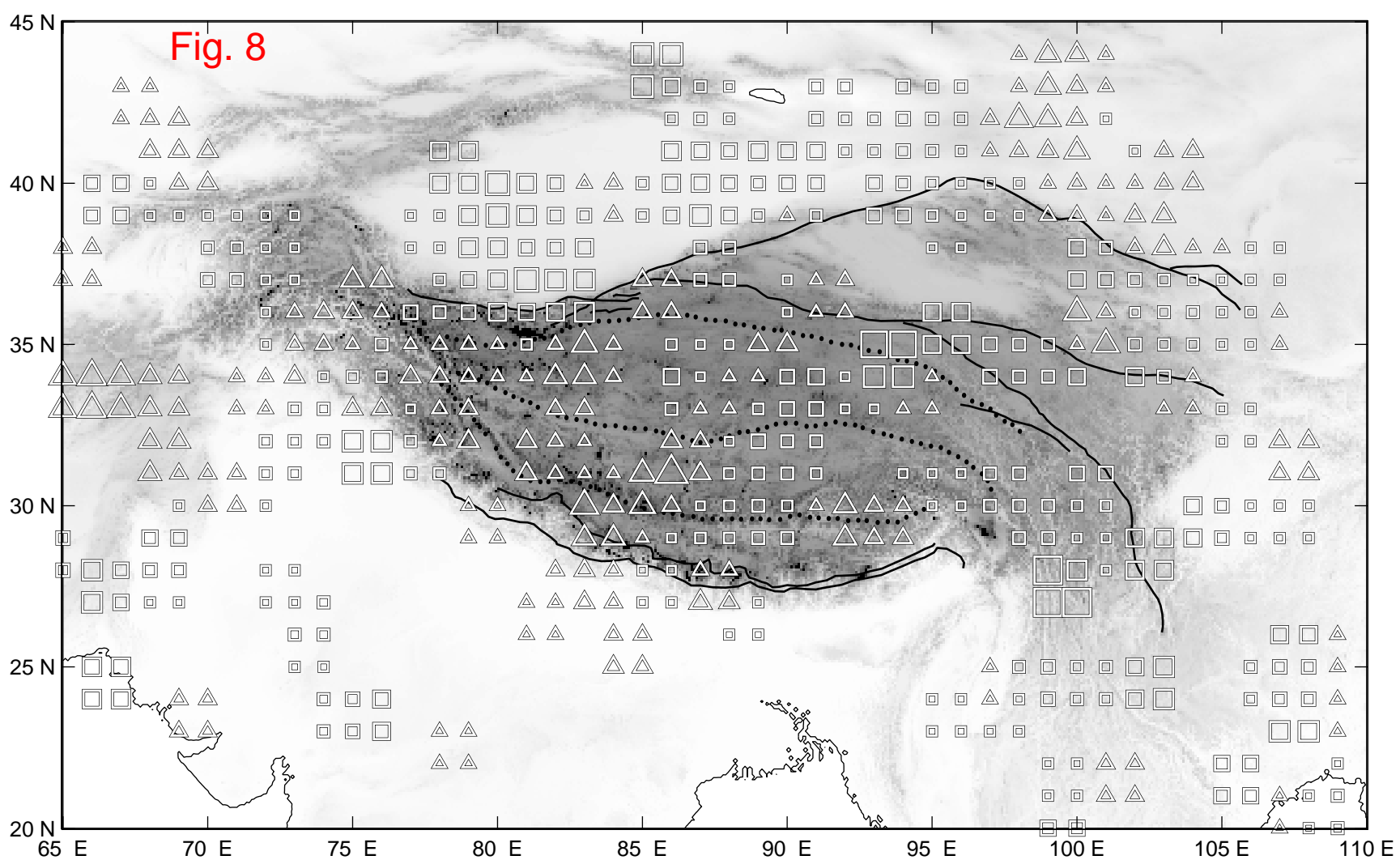
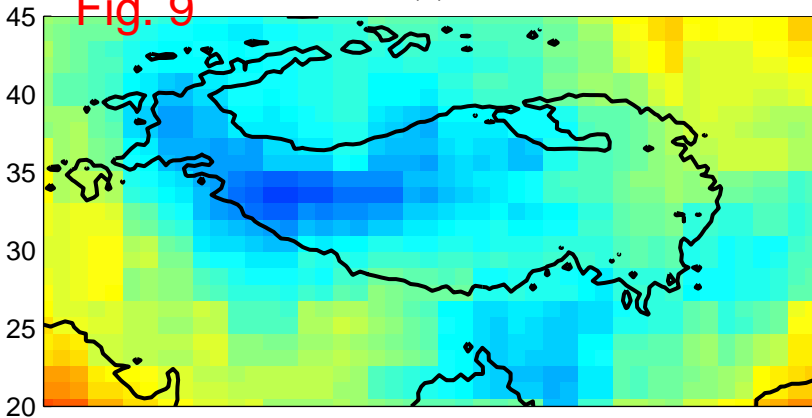
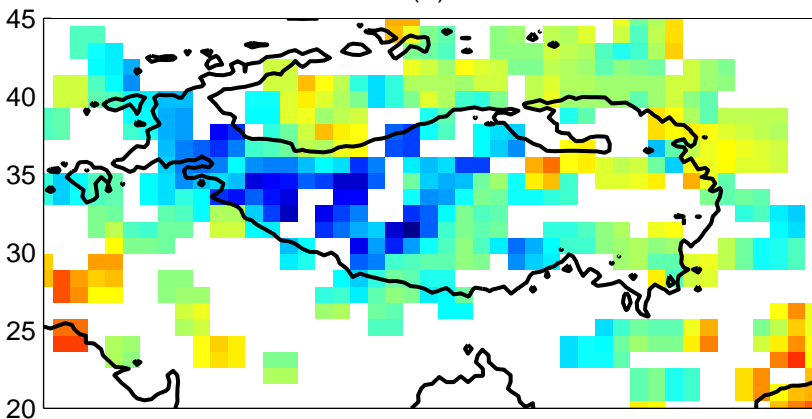


Fig. 9

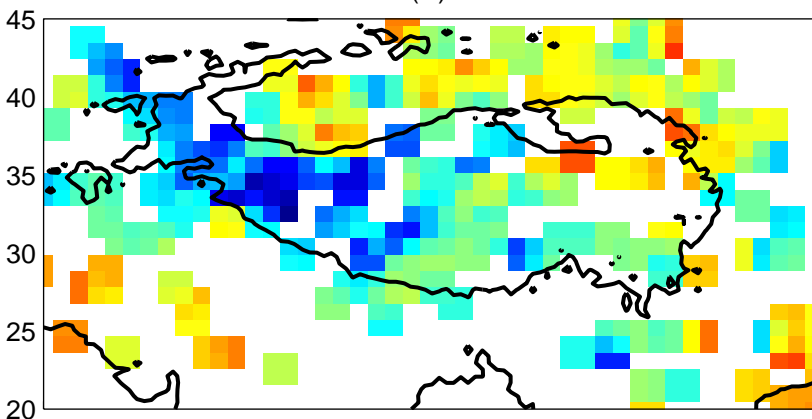
(A)



(B)



(C)



PREM



4.4 4.5 4.6 4.7 4.8 4.9 5 5.1

S wave speed, km/s

